COMPARISON OF THE AUSM$^+$ AND H-CUSP SCHEMES FOR TURBOMACHINERY APPLICATIONS

R. V. Chima and M.–S. Liou
NASA Glenn Research Center
Brook Park, Ohio 44135

Abstract

Many turbomachinery CFD codes use second-order central-difference (C-D) schemes with artificial viscosity to control point decoupling and to capture shocks. While C-D schemes generally give accurate results, they can also exhibit minor numerical problems including overshoots at shocks and at the edges of viscous layers, and smearing of shocks and other flow features. In an effort to improve predictive capability for turbomachinery problems, two C-D codes developed by Chima, RVCQ3D and Swift, were modified by the addition of two upwind schemes: the AUSM$^+$ scheme developed by Liou, et al., and the H-CUSP scheme developed by Tatsumi, et al. Details of the C-D scheme and the two upwind schemes are described, and results of three test cases are shown. Results for a 2-D transonic turbine vane showed that the upwind schemes eliminated viscous layer overshoots. Results for a 3-D turbine vane showed that the upwind schemes gave improved predictions of exit flow angles and losses, although the H-CUSP scheme predicted slightly higher losses than the other schemes. Results for a 3-D supersonic compressor (NASA rotor 37) showed that the AUSM$^+$ scheme predicted exit distributions of total pressure and temperature that are not generally captured by C-D codes. All schemes showed similar convergence rates, but the upwind schemes required considerably more CPU time per iteration.

Introduction

Turbomachinery blades are usually designed with proprietary design codes and are heavily analyzed with computational fluid dynamics (CFD) codes before committing to manufacture. However, turbomachinery designers often distrust absolute performance predictions and rely only on changes in predicted performance between designs. This practice suggests that the accuracy of CFD codes can still be improved.

In 1994 ASME and IGTI sponsored a blind test case for turbomachinery CFD codes at the 39th International Gas Turbine Conference held in The Hague (unpublished.) The same test case was later adopted by the AGARD Propulsion and Energetics Panel Working Group 26 as a test case for examining effects of grid and turbulence model on solution accuracy.[1,2] Sixteen different CFD codes were used to predict the performance of a transonic compressor rotor designated NASA rotor 37.[3,4] One operating point at 98 percent of maximum flow was examined in detail. Predicted pressure ratios varied by nearly 10 percent, and predicted efficiencies varied by about 6 points. In general, pressure ratios were too high and the efficiencies were too low. The large variations in results again suggests that the codes can still be improved.

Most of the codes used for these test cases used second-order central-difference (C-D) schemes with artificial viscosity to control point decoupling and to capture shocks. While C-D schemes generally give accurate answers, they can also exhibit some minor numerical problems. Shock smearing and overshoots are well known and can be minimized by switching off fourth-difference dissipation at shocks. Overshoots at the edge of viscous layers are less well known but were shown in refs. 5 and 6. Many researchers have speculated that artificial viscosity may smear out other flow features, but this can be difficult to demonstrate.

Other work has shown that improved artificial viscosity schemes or upwind schemes can give better accuracy than standard C-D schemes. In ref. 5 Tweedt, Chima, and Turkel compared two artificial viscosity schemes in a C-D code. The first was a standard artificial viscosity scheme with blended second and fourth differences and Eigenvalue scaling.[7–9] The second was the Symmetric Limited Positive (SLIP) flux limiter which is the low-speed part of the more general Convective Upward Split Pressure (CUSP) schemes developed by Tatsumi, Martinelli, and Jameson.[10,11] It was shown that the SLIP formulation gave better resolution of laminar boundary layer velocity profiles and better predictions of performance of a low-speed centrifugal impeller than the standard formulation.

In several papers, Liou and others have developed the Advection Upstream Splitting Method (AUSM) family of upwind schemes and applied them to many

aerodynamic problems ranging from 1-D shock tube problems to 3-D multi-element wings.[12–15] These applications have shown that the AUSM schemes have excellent shock-capturing properties and give very accurate results for a wide variety of problems.

In the present work the H-CUSP and AUSM$^+$ schemes were added to two C-D turbomachinery analysis codes developed by Chima, RVCQ3D[6,16] and Swift.[17–19] Three turbomachinery blades were analyzed and the results were compared to experimental data. In each case the upwind schemes gave significant improvements over the C-D scheme. Results for a 2-D transonic turbine vane showed that the upwind schemes eliminated viscous layer overshoots. Results for a 3-D turbine vane showed improvements in predicted exit flow angle and loss profiles with the upwind schemes. Finally, results for a 3-D supersonic compressor (NASA rotor 37) showed that the AUSM$^+$ scheme gave large improvements in the prediction of exit total pressure and total temperature profiles.

CFD Codes

Swift

The Swift code is a multiblock Navier-Stokes analysis code for turbomachinery blade rows.[17–19] The code solves the Navier-Stokes equations on body-fitted grids using an explicit finite-difference scheme. It includes viscous terms in the blade-to-blade and hub-to-tip directions, but neglects them in the streamwise direction using the thin-layer approximation. Two turbulence models were used: the Baldwin-Lomax model,[20] and Wilcox's k-ω model[6,21] with Menter's shear stress transport (SST) modification.[22]

The baseline code used C-D's for the fluxes, and scalar artificial dissipation to capture shocks and to control point decoupling.[17] Eigenvalue scaling was used to scale the artificial dissipation directionally on stretched grids.[8,9] An explicit, four-stage Runge-Kutta scheme[7] was used to solve the flow equations. To accelerate convergence to a steady state, all calculations were run at a Courant numbers around 5.6 using a spatially-varying time step and implicit residual smoothing. The Eigenvalue scaling was also used to scale the implicit smoothing coefficients.

RVCQ3D

The quasi-three-dimensional turbomachinery analysis code RVCQ3D developed by Chima[6,16] was used to develop and test the upwind schemes before attempting 3-D calculations. RVCQ3D solves the thin-layer Navier-Stokes equations on a blade-to-blade plane. Radius change, stream surface thickness, and rotation can all be modeled. The differencing scheme, artificial dissipation, and solution algorithms were all similar to those described previously for the Swift code.

Governing Equations

The Navier-Stokes equations were written in a Cartesian (x, y, z) coordinate system rotating about the x-axis with angular velocity Ω. The equations were transformed to a curvilinear (ξ, η, ς) system using standard techniques, and all viscous terms in the ξ-direction were dropped using the thin-layer approximation. The resulting equations are:

$$\partial_t q + J[\partial_\xi E + \partial_\eta F + \partial_\varsigma G - Re^{-1}(\partial_\eta F_v + \partial_\varsigma G_v)] = H \quad (1)$$

where $q = [\rho, \rho u, \rho v, \rho w, e]^T$ is the vector of conservation variables, and

$$E = J^{-1}\begin{bmatrix} \rho U' \\ \rho u U' + \xi_x p \\ \rho v U' + \xi_y p \\ \rho w U' + \xi_z p \\ \rho h_0 U' + \Omega \xi_\theta p \end{bmatrix} \quad (2)$$

etc. are the inviscid fluxes, F_v and G_v are viscous fluxes, and H is a source term due to rotation. In (1) and (2) $e = \rho\left[C_v T + \frac{1}{2}(u^2 + v^2 + w^2)\right]$ is the total internal energy and $h_0 = (e + p)/\rho$ is the total enthalpy. The full equations are given in ref. 17.

In equation (2) U' is the contravariant velocity component in the *relative* frame of reference. Using primes to denote relative velocities,

$$\begin{aligned} U' &= \xi_x u + \xi_y v' + \xi_z w' \\ v' &= v - \Omega z \\ w' &= w + \Omega y \end{aligned} \quad (3)$$

Rearranging terms gives

$$\begin{aligned} U' &= (\xi_x u + \xi_y v + \xi_z w) - \Omega(\xi_y z - \xi_z y) \\ &= U - \Omega \xi_\theta \end{aligned} \quad (4)$$

Metric terms ξ_x, etc. are evaluated at grid points using a conservative, centered scheme.[5] The metric terms (including ξ_θ) are averaged to $i \pm 1/2$ for the upwind schemes. The Jacobian term J can usually be

combined with the metric terms and will be neglected here.

Equation (1) is solved in the following form:

$$\partial_t q = -J[R_i - (R_v + D)] \tag{5}$$

where R_i is the inviscid residual, R_v is the viscous residual, and D is a numerical dissipation operator.

Artificial Dissipation and Upwind Schemes

Baseline Scheme

The baseline numerical scheme uses standard central differences for the flux terms $\partial_\xi E$, and a scalar artificial dissipation D. D is written as the sum of a second and forth difference operator in each direction:

$$\begin{aligned} Dq &= (D_\xi + D_\eta + D_\varsigma)q \\ D_\xi q &= \partial_\xi[C_\xi(\varepsilon_2 \partial_\xi q - \varepsilon_4 \partial_{\xi\xi\xi} q)] \end{aligned} \tag{6}$$

where ε_2 and ε_4 are coefficients given by

$$\begin{aligned} \varepsilon_2 &= K_2 max(\nu_{i-1}, \nu_i, \nu_{i+1}, \nu_{i+2}) \\ \varepsilon_4 &= max(0, K_4 - \varepsilon_2) f_i \\ K_2 &= 1/4 \\ K_4 &= (0.25 \text{ to } 1)/16 \end{aligned} \tag{7}$$

ν_i is a pressure sensor for shocks

$$\nu_i = \frac{|p_{i-1} - 2p_i + p_{i+1}|}{|p_{i-1} + 2p_i + p_{i+1}|} \tag{8}$$

and f_i is a ramping function that reduces the dissipation linearly with grid index near solid surfaces (typically by a factor of 0.05 at the wall) to minimize effects on skin friction.

Experience has shown that more dissipation is often needed along the long side of highly-stretched cells. Thus equation (6) includes an Eigenvalue scaling coefficient C_ξ, originally proposed by Martinelli, et al.[8] Here a modification proposed by Kunz, et al.[9] was used.

$$\begin{aligned} C_\xi &= \lambda_\xi \sqrt{1 + \frac{\lambda_\eta + \lambda_\varsigma}{\lambda_\xi}} \\ \lambda_\xi &= |U'| + c\xi_s \\ \xi_s &= \sqrt{\xi_x^2 + \xi_y^2 + \xi_z^2} \end{aligned} \tag{9}$$

In (9,) λ_ξ is the maximum Eigenvalue (i.e., the spectral radius) of the inviscid flux Jacobian, c is the speed of sound, and ξ_s is the inverse of the spacing normal to the surface.

H-CUSP Scheme

The Symmetric Limited Positive (SLIP) scheme was introduced by Tatsumi, Martinelli, and Jameson in refs. 10 and 11. The scheme uses flux-limited dissipation to produce a non-oscillatory scheme.

The Convective Upward Split Pressure (CUSP) scheme was also introduced in refs. 10 and 11. The CUSP scheme was developed as a flux-split scheme similar to the AUSM scheme; however, it was implemented as a dissipative flux added to a C-D flux. For computational efficiency the dissipative fluxes can be updated less often than the C-D fluxes. The E-CUSP formulation bases the dissipative fluxes on the internal energy, while the H-CUSP formulation is based on stagnation enthalpy. The H-CUSP formulation was used here.

For the H-CUSP scheme, the artificial dissipation is written as:

$$D_\xi q = (d_{i+1/2} - d_{i+1/2})q \tag{10}$$

where

$$d_{i+1/2} = \frac{1}{2}\alpha^* c\xi_s (q_R - q_L) + \frac{1}{2}\beta(E_R - E_L) \tag{11}$$

The first term is a difference of the conservation variables q. If $q_R = q_{i+1}$ and $q_L = q_i$, the term becomes a first-order artificial dissipation. If q_R and q_L are evaluated using the SLIP limiter described later, the term becomes third order in smooth regions of the flow and first order near shocks, similar to baseline scheme. The second term is a difference of the fluxes E. It is added to give a true upwind scheme for supersonic flow. Switching terms α^* and β are devised to use the first term for low speeds and the second term for $M > 1$, with a continuous blending in between.

Liou and Steffen proposed a decomposition of the flux E into a convective term and a pressure term.[12] An equivalent splitting is used for the CUSP schemes.

$$\begin{aligned} E &= U'\psi + pg \\ \psi &= [\rho, \rho u, \rho v, \rho w, \rho h_0]^T \\ g &= \left[0, \xi_x, \xi_y, \xi_z, \Omega\xi_\theta\right]^T \end{aligned} \tag{12}$$

Using this decomposition, (11) becomes:

$$d_{i+1/2} = \frac{1}{2}\alpha^* c\xi_s(q_R - q_L) + \frac{1}{2}\beta[(U_R'\psi_R - U_L'\psi_L) + g_{i+1/2}(p_R - p_L)] \quad (13)$$

An interface relative Mach number is defined by:

$$M = \frac{\tilde{U}'}{\tilde{c}\xi_s} \quad (14)$$

where the tilde indicates Roe averaging,

$$\tilde{u} = \frac{\sqrt{\rho_L}u_L + \sqrt{\rho_R}u_R}{\sqrt{\rho_L} + \sqrt{\rho_R}}, \text{ etc., and}$$
$$\tilde{c} = \sqrt{(\gamma - 1)\left(\tilde{h}_0 - \frac{1}{2}(\tilde{u}^2 + \tilde{v}^2 + \tilde{w}^2)\right)}. \quad (15)$$

Then the switching function β is given by:

$$\beta = \begin{cases} max(0, 2M - 1) & \text{for } 0 \le M \le 1 \\ min(0, 2M + 1) & \text{for } -1 \le M \le 0 \\ sign(M) & \text{for } |M| \ge 1 \end{cases} \quad (16)$$

which can be coded conveniently as

$$f_M = 2|M| - 1$$
$$\beta = sign(1, M) \times min[1, max(0, f_M)]. \quad (17)$$

Tatsumi, et al. showed that one-point shocks could be obtained if switching function $\alpha^* c$ is given by:

$$\alpha^* c = \alpha\tilde{c} - \beta\tilde{U}' \quad (18)$$

where

$$\alpha = r^+ max(|M|, r^- M_0)$$
$$r^+ = max[1, (1 - 2|M|)r_\xi]$$
$$r^- = min(1, r_\xi)$$
$$r_\xi = (C_\eta + C_\varsigma)/C_\xi \quad (19)$$

M_0 is a cutoff Mach number, typically taken as $M_0 \sim 0.1 \times min(1, M_{\max})$, where M_{max} is the largest relative Mach number expected in the flow field. Swanson, et al. showed that the CUSP schemes also benefit from increased dissipation along the long side of stretched cells.[23] They suggested Eigenvalue scaling terms r^+ and r^-. Here r^+ has been modified by the addition of the $(1 - 2|M|)$ term. Coefficients α and β are shown in figure 1.

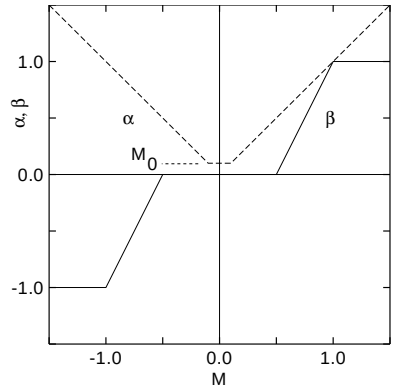

Figure 1 — Functions α and β for the H-CUSP scheme

AUSM$^+$ Scheme

The Advection Upstream Splitting Method (AUSM) scheme was introduced by Liou and Steffen in 1991.[12] The AUSM scheme defines a cell interface Mach number based on characteristic speeds from the neighboring cells. The interface Mach number is used to determine the upwind extrapolation for the convective part of the inviscid fluxes. A separate splitting is used for the pressure terms. Generalized Mach number and pressure splitting functions were described by Liou[13] and the new scheme was termed ASUM$^+$. The AUSM$^+$ scheme was shown to have several desirable properties: 1, it gives exact resolution of 1-D contact and shock discontinuities, 2, it preserves positivity of scalar quantities, and 3, it is free of oscillations at stationary and moving shocks.

The AUSM$^+$ scheme avoids an explicit artificial dissipation, and differences the fluxes directly using:

$$\partial_\xi E = E_{i+1/2} - E_{i-1/2} \quad (20)$$

A flux decomposition similar to (12) is used to write

$$E = \rho U'\phi + pg$$
$$\phi = \psi/\rho = [1, u, v, w, h_0]^T \quad (21)$$

Here $\rho U'$ is the mass flux across a cell interface. It can be written as:

$$\dot{m} = \rho U' = \rho\bar{c}\xi_s\frac{U'}{\bar{c}\xi_s} = \rho\bar{c}\xi_s M \quad (22)$$

where $\bar{c} = (c_R + c_L)/2$ is the average speed of sound, and M is the relative interface Mach number.

The fluxes are differenced using:

$$E_{i+1/2} = \begin{cases} \rho_L \tilde{c} \xi_s M_{i+1/2} \phi_L + g p_{i+1/2} & \text{if } M_{i+1/2} \geq 0 \\ \rho_R \tilde{c} \xi_s M_{i+1/2} \phi_R + g p_{i+1/2} & \text{else} \end{cases} \quad (23)$$

where ξ_S and g are evaluated at $i+1/2$. Note that the average speed of sound $\bar{c}$ has been replaced with a numerical speed of sound $\tilde{c}$ which is described later.

The interface Mach number and pressure are evaluated using weighted averages of the left and right states. Defining left and right Mach numbers based on $\tilde{c}$ as:

$$M_{L,R} = \left(\frac{U'}{\tilde{c} \xi_s} \right)_{L,R} \quad (24)$$

then $M_{i+1/2}$ and $p_{i+1/2}$ are given by:

$$\begin{aligned} M_{i+1/2} &= M^+ + M^- + D_p \\ p_{i+1/2} &= P^+ p_L + P^- p_R + D_v \end{aligned} \quad (25)$$

$M^{\pm}$ and $P^{\pm}$ are functions of M_L and M_R:

$$\begin{array}{lll} \text{if } |M_L| < 1 & M^+ = M_{2L}, & P^+ = P_{5L} \\ \text{else} & M^+ = M_{1L}, & P^+ = M_{1L}/M_L \\ \text{if } |M_R| < 1 & M^- = M_{2R}, & P^- = P_{5R} \\ \text{else} & M^- = M_{1R}, & P^- = M_{1R}/M_R \end{array} \quad (26)$$

$M_{2(L,R)}$ are second order polynomials in $M_{L,R}$:

$$M_{2L} = \frac{1}{4}(M_L + 1)^2 \qquad M_{2R} = -\frac{1}{4}(M_R - 1)^2, \quad (27)$$

$M_{1(L,R)}$ are directional switching functions:

$$M_{1L} = max(M_L, 0) \qquad M_{1R} = min(M_R, 0), \quad (28)$$

and $P_{5(L,R)}$ are fifth order polynomials in $M_{L,R}$:

$$\begin{aligned} P_{5L} &= M_{2L}(2 - M_L) + \frac{3}{16} M_L (M_L^2 - 1)^2 \\ P_{5R} &= -M_{2R}(2 + M_R) - \frac{3}{16} M_R (M_R^2 - 1)^2 \end{aligned} \quad (29)$$

Plots of $M^{\pm}$ and $P^{\pm}$ are shown in figure 2.

The AUSM schemes define the mass flux across a cell interface in terms of split Mach numbers and a common interface speed of sound, $\bar{c}$ in equation (22.) However, Liou and Edwards showed that the interface speed of sound $\tilde{c}$ in equation (24) could be chosen arbitrarily without affecting the shock-capturing properties of the

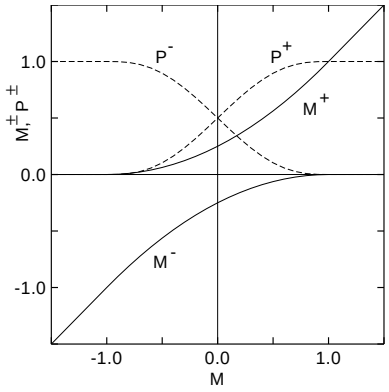

Figure 2 — Functions $M^{\pm}$ and $P^{\pm}$ for the AUSM$^+$ scheme

scheme.[14] They proposed using a "numerical speed of sound" that effectively scales the numerical dissipation with the local flow speed $|u|$ instead of the local sound speed c as $M \to 0$. In other words, the numerical speed of sound goes to zero with the local Mach number. They showed that the numerical speed of sound gave appropriate amounts of dissipation, even when used with preconditioning methods at very low speeds.

The numerical speed of sound is given by:

$$\begin{aligned} \tilde{c} &= f \bar{c} \\ f &= \frac{\sqrt{(1 - M_*^2)\overline{M}^2 + 4M_*^2}}{1 + M_*^2} \\ \overline{M} &= \frac{1}{2}(M_L + M_R) \\ M_* &= min[1, max(|\overline{M}|, M_0)] \end{aligned} \quad (30)$$

where f is a scaling factor, $\overline{M}$ is an average interface Mach number, and M_* is the local relative Mach number limited between a cutoff Mach number M_0 and 1. M_0 is typically taken as $(0.2 \text{ to } 0.5) \times min(M_{max}, 1)$.

In equations (25,) D_p and D_v are diffusive terms that have been introduced to ensure pressure-velocity coupling at low speeds. D_p is a pressure-diffusion term that was introduced by Liou and Edwards.[14] The term was originally added to the mass flux, but here it was recast as a modification to $M_{i+1/2}$, and all density terms were cancelled. The term was also reduced by a factor of two by numerical experimentation. The result is:

$$D_p = \frac{1}{4}\frac{\Delta M(p_L - p_R)}{M_*^2(p_L + p_R)}$$
$$\Delta M = (M_{2L} - M_{1L}) - (M_{2R} - M_{1R}) \quad (31)$$

Finally D_v is a velocity-diffusion term that was introduced by Liou.[15] It is given by:

$$D_v = -P^+P^-\left(\frac{\rho_L + \rho_R}{2}\right)\tilde{c}^2(M_R - M_L) \quad (32)$$

Limiters

SLIP Limiter

For the H-CUSP scheme the right and left states were calculated using the SLIP limiter.[10] For left and right states *a* and *b*, the limiter is defined by:

$$R(a, b) = 1 - \left|\frac{a - b}{|a| + |b|}\right|^2, \quad (33)$$

and a limited average is defined by

$$L(a, b) = R(a, b)\left(\frac{a + b}{2}\right). \quad (34)$$

The conservation variables q are interpolated to $i \pm 1/2$ using:

$$q_L = q_i + \frac{1}{2}L(\Delta q_{i-1/2}, \Delta q_{i+3/2})$$
$$q_R = q_{i+1} + \frac{1}{2}L(\Delta q_{i-1/2}, \Delta q_{i+3/2}) \quad (35)$$
$$\Delta q_{i-1/2} = q_i - q_{i-1}$$

van Albada Limiter

For the AUSM$^+$ scheme the right and left states were calculated using the van Albada limiter.[24] The limiter is defined by:

$$S(a, b) = \frac{(a^2 + \varepsilon)v + (b^2 + \varepsilon)u}{(a^2 + \varepsilon) + (b^2 + \varepsilon)} \quad (36)$$

where $\varepsilon = 10^{-7}$. The primitive variables $\omega = \left[\rho, u, v, w, p\right]^T$ are interpolated to $i \pm 1/2$ using:

$$\omega_L = \omega_i + \frac{1}{2}S(\Delta\omega_{i-1/2}, \Delta\omega_{i+1/2})$$
$$\omega_R = \omega_{i+1} - \frac{1}{2}S(\Delta\omega_{i-1/2}, \Delta\omega_{i+1/2}) \quad (37)$$

SST k-ω Turbulence Model

Results for a transonic compressor rotor shown later used the SST k-ω turbulence model. Wilcox's baseline k-ω model was described in ref. 21, and the implementation of the model in RVCQ3D was described in ref. 6. The shear stress transport (SST) model was developed by Menter in ref. 22, and is described below.

The SST model is based on Bradshaw's assumption that the shear stress in a boundary layer is proportional to *k*. Menter showed that this could be added to the baseline model as a modification to the turbulent viscosity.

$$\nu_t = \frac{a_1 k}{max(a_1\omega, \Omega F_2)} \quad (38)$$

where $a_1 = 0.3$, and Ω is the magnitude of the vorticity. The first term in the denominator recovers the baseline model and the second term gives the SST model. Since Bradshaw's assumption does not necessarily hold in free-shear layers, F_2 is a blending function that turns the SST model off away from the wall.

$$F_2 = \tanh(\arg_2^2)$$
$$\arg_2 = max\left(\frac{2\sqrt{k}}{0.09\omega y}, \frac{400\nu}{\omega y^2}\right) \quad (39)$$

Menter has shown that the SST model gives excellent results for adverse pressure gradients. The one disadvantage to the model is that it requires the distance to the wall *y*.

Results

2-D Transonic Turbine Vane

A transonic turbine vane tested by Arts, et al.[25] was computed as a 2-D test case. The vane was tested experimentally in the Isentropic Light Piston Compression Tube Facility at the von Karman Institute. The facility has independent control over the exit Reynolds number, the exit isentropic Mach number, $M_{2,is}$, and the inlet turbulence intensity. Surface pressures were measured with static taps, and wake total pressure profiles were measured with a high-speed traversing probe.

For the computations a C-type grid was used with 383×49 (C, y) points. The grid spacing gave $y^+ < 1.5$ over most of the vane. The grid size was found to give good resolution of the suction surface shock and surface heat transfer in ref. 6. Solutions were run for a case with an exit Mach number of $M_{2,is} = 1.0$ using the C-D, H-CUSP, and the AUSM$^+$ schemes and the Baldwin-

Lomax turbulence model. All solutions were run using a 4-stage Runge-Kutta scheme at a Courant number of 5.6. Dissipative terms were evaluated after the first stage, and the turbulence model was updated every five iterations. Convergence rates were similar for all schemes, with mass flow error and total pressure loss converged to 0.3 percent or better in 2000 iterations. On an SGI Octane workstation the C-D solution took 188 sec. The H-CUSP solution took 1.27 times longer, and the AUSM$^+$ solution took 2.65 times longer than the C-D scheme.

Computed Mach contours are shown in fig. 3. The heavy black line is $M = 1.0$ and the contour increment is 0.05. The flow accelerates from $M = 0.15$ at the inlet to $M = 1.2$ on the suction surface. A normal shock reduces the Mach number to $M \approx 1.0$ at the exit. Enlargements of the shock, trailing edge, and wake computed with the three different schemes are shown in fig. 4. The C-D results show some oscillations around the shock and more severe oscillations around the wake. The H-CUSP scheme eliminates most of the oscillations, although some are visible in the core flow. The AUSM$^+$ results show a very clean shock and are completely non-oscillatory.

Computed distributions of isentropic surface Mach number are compared to experimental data in fig. 5.† All schemes agree very well with the experimental data.

Computed wake profiles located 43 percent of axial chord downstream of the trailing edge are compared to the experimental data (digitized manually from ref. 25) in fig. 6. The C-D results show the same oscillations in total pressure at the edge of the wake that were seen in the contour plots in fig. 4. Neither of the upwind schemes shows oscillations. The AUSM$^+$ results agree very well with the experimental data, but the H-CUSP results show slightly too much wake decay and free-stream loss.

3-D Subsonic Turbine Vane

An annular turbine vane that was tested experimentally by Goldman and McLallin at NASA Glenn Research Center[26] was used as a 3-D turbine test case. A C-type computational grid was used, with $97 \times 32 \times 33$ (C, θ, r) points. The grid spacing gave $y^+ = O(5)$ over most of the vane. Although the grid was rather coarse, it gave reasonably accurate predictions of vane performance with quick turnaround. Solutions were run using the C-D, H-CUSP, and the AUSM$^+$ schemes and the Baldwin-Lomax turbulence model. The iterative scheme was the same as that used for the 2-D case. Convergence rates were similar for all schemes, with the maximum residual reduced about four orders of magnitude in 1500 iterations. Total pressure losses were converged to four digits.

The solutions were run on the Cray SV1ex computer at NASA Ames Research Center (Bright.) The C-D solution took about 1/2 hour, or about six minutes of wall clock time using six processors. The H-CUSP scheme took 1.47 times longer than the C-D scheme, and the AUSM$^+$ scheme took 1.57 times longer than the C-D scheme.

Computed pressure contours on the blade surfaces are shown in fig. 7. The blade profile is uniform along the span, and the pressure distribution is nearly uniform. The flow accelerates from $M = 0.21$ at the inlet to $M = 0.73$ at the exit.

Figure 8 compares measured and calculated contours of kinetic energy efficiency across the wake at a distance of 1/3 axial chord downstream of the trailing edge. The kinetic energy efficiency is defined by:

$$\eta = \frac{Q^2}{2C_p(T_0 - T)} \tag{40}$$

where Q is the velocity, T_0 is the total temperature, and T is the static temperature. The C-D scheme smears many of the details of the wake. The H-CUSP scheme captures the wake shape better, showing underturned, high loss regions near the endwalls due to secondary flows. The AUSM$^+$ scheme overexaggerates the wake shape; however, subsequent results will show that the AUSM$^+$ scheme gives the best quantitative agreement with experiment.

The spanwise variation of mixed out total pressure loss coefficient $1 - P_{0ex}/P_{0in}$ downstream of the vanes is shown in fig. 9. The C-D results show little detail along the span. The H-CUSP results show some detail near the tip but too much loss near the hub. The AUSM$^+$ results show good qualitative agreement with the data along the entire span. All results show higher losses than the data at midspan. The midspan loss does not improve with increasing grid resolution, and may be due to poor modeling of the round trailing edge.

The spanwise variation of flow angle downstream of the vanes is shown in fig. 10. The C-D results show nearly uniform flow angle along the span, and the H-

†. In all figures the C-D results are labeled “Baseline” and are shown with a solid black line, AUSM$^+$ results are shown with a dashed red line, and H-CUSP results are shown with a dotted blue line.

CUSP results are only slightly better. The AUSM$^+$ results show excellent agreement with the data along the entire span.

3-D Compressor Rotor

A low aspect ratio transonic inlet rotor for a core compressor, designated NASA rotor 37, was used as a 3-D compressor test case. The rotor was originally designed and tested at NASA Glenn Research Center in the late 1970's by Reid and Moore.[3,4] It has 36 multiple-circular-arc blades and a design pressure ratio of 2.106 at a mass flow of 20.19 kg/sec.

The rotor was re-tested in a single-stage compressor facility at NASA Glenn. The test facility was described by Suder, et al.[27,28] Radial distributions of static and total pressure, total temperature, and flow angle were measured at two axial stations located 4.19 cm upstream and 10.19 cm downstream of the blade hub leading edge.

These measurements were used for the ASME/IGTI blind test case and the AGARD test case for turbomachinery CFD codes.[1,2] Calculations from sixteen different CFD codes were compared to the measurements. Two details of the measurements proved to be difficult to predict: First, most codes overpredicted the overall pressure and temperature ratios, and underpredicted the efficiency. Second, most codes failed to predict the radial distributions of P_0 and T_0 downstream of the rotor. Measured distributions show deficits in these quantities near 20 percent span, but most codes showed fairly linear radial distributions.

Two researchers predicted these distributions correctly: Hah using his HAH3D code with a pressure-based, high-order upwind difference scheme and a k-ε turbulence model,[29] and Weber using the OVERFLOW code with a Roe upwind scheme and the Spalart-Almaras turbulence model.[1,2] Most of the other codes used for the test case used C-D schemes with artificial viscosity and a variety of turbulence models.

Hah believed that the deficits in total conditions were due to a corner stall.[29] Alternatively, Shabbir, et al. proposed that flow leakage between the centerbody and rotor disk could generate enough blockage to produce the deficits.[30] In this paper we suggest that the C-D schemes used in most codes smear details of the P_0 and T_0 distributions, while the upwind schemes used previously by Hah and Weber, and now in this work provide increased accuracy that gives better agreement with the experimental data.

A multiblock grid was used for the present calculations (fig. 11.) An H-type grid was used upstream of the blade with $45 \times 34 \times 63$ (x, θ, r) points. A periodic C-type grid was used around the blade with $259 \times 46 \times 63$ points. The grid spacing at the blade and endwalls was 4×10^{-4} cm, giving $y^+ = 2 - 4$ at the surfaces. The blade-to-blade grid was optimized in a grid refinement study performed for the ASME/IGTI blind test case (unpublished.) The inlet and exit of the grid were coincident with the measurement stations described earlier. An O-type grid was used above the tip of the blade with $199 \times 13 \times 13$ points (13 points across the gap.) The total grid had 869,011 points, which is 3–4 times finer than the grids recommended by Dunham, et al.[2]

C-D/Baldwin-Lomax calculations were run previously for the ASME blind test case.[18] Some of these results are included later for comparison.

The present results were computed using the SST k-ω turbulence model. Preliminary results using the baseline k-ω model showed that the AUSM/k-ω scheme predicted higher pressure ratios than the AUSM/Baldwin-Lomax scheme. The reason was unclear, but seemed to be related to better resolution of the shock/boundary layer interaction on the casing. Menter's SST k-ω model was then added to the baseline k-ω model. Pressure ratios predicted with the AUSM/SST k-ω scheme agreed closely with the AUSM/Baldwin-Lomax results and are presented here.

The ASUM$^+$ scheme was used to calculate several operating points. The C-D and H-CUSP schemes were each used to compute one operating point at 98.7 percent max flow. All calculations were run with a four-stage Runge-Kutta scheme at a Courant number of 5.5. Artificial and physical dissipation terms were evaluated at stages 1 and 2. The turbulence model was updated every two iterations. The calculations were typically run $3,000$ iterations to ensure convergence of the mass flow error and total pressure ratio to about 0.01 percent. The total CPU time on the Cray SV1ex computer was about 10 hours per case for the C-D scheme, but on six processors the wall clock time was roughly 1.8 hours. The H-CUSP scheme took 1.20 times longer than the C-D scheme, and the AUSM$^+$ scheme took 1.24 times longer than the C-D scheme.

Figure 12 shows computed contours of relative Mach number at 73 percent span at 98.7 percent max flow. The heavy black contour is $M = 1$ and the contour increment is 0.05. An oblique shock system runs upstream of the blade and across the passage, where it

merges with a normal shock. AUSM$^+$ results are shown, but the C-D and H-CUSP results look similar.

Computed maps of total pressure ratio, total temperature ratio, and adiabatic efficiency versus mass flow are shown in fig. 13. The dotted black line shows the C-D/Baldwin-Lomax results reported in ref. 18, with the one CD/SST k-ω result added. The blue triangles show the H-CUSP solution, and the red triangles show the AUSM$^+$ solutions. No attempt was made to determine the numerical stall point with the AUSM$^+$ scheme. All schemes overpredict the pressure and temperature ratios, but give very good predictions of the adiabatic efficiency.

Figures 14 – 16 compare radial profiles of total pressure, total temperature, and adiabatic efficiency downstream of the rotor with experimental data taken at 98 percent of the maximum flow rate. Hah, et al. showed that these profiles were very sensitive to the flow rate,[29] and that much better agreement was obtained by comparing calculations at about 99 percent flow. The solutions shown here are all at a flow rate around 98.7 percent max flow.

Total pressure profiles are shown in fig. 14. The data shows the deficit in P_0 below 30 percent span that most codes in the ASME/AGARD test case were unable to predict. Here the H-CUSP results show a nearly linear distribution of P_0 along the span that still fits the data well overall. The baseline C-D results are similar near the tip but show an overshoot near the hub. The AUSM$^+$ results match the data very well except for a slight overshoot at the hub. Many of the codes in the ASME/AGARD test case showed similar overshoots near the hub.

Total temperature profiles are shown in fig. 15. The C-D results are smooth along the span and do not match the shape of the measured profile very well. The H-CUSP results are similar, but give slightly better resolution of the profile shape. The AUSM$^+$ results agree very closely with the data between 15 and 85 percent span. The three schemes give minor differences in predicted T_0 near the hub that are consistent with the overshoots in P_0 noted above. All three schemes overpredict T_0 near the tip, which accounts for the high overall temperature (and pressure) ratios in fig. 13. Almost every code in the ASME/AGARD test case also overpredicted T_0 near the tip, and the reason remains unknown.

Adiabatic efficiency profiles are shown in fig. 16. Here all three schemes give remarkably similar results that agree very well with the data below 85 percent span. This indicates that loss levels are being predicted correctly by the SST k-ω turbulence model, except perhaps near the casing.

Conclusions

Two centrally-differenced (C-D) turbomachinery analysis codes developed by Chima, RVCQ3D and Swift, were modified by the addition of two upwind schemes: the AUSM$^+$ scheme developed by Liou, et al. and the H-CUSP scheme developed by Tatsumi, et al. Several test cases were run to evaluate the effects of the differencing schemes on turbomachinery flow predictions. The upwind schemes gave improvements in the predictions over the C-D scheme for every case investigated. The following results were noted:

1. The C-D scheme produced overshoots at the edge of viscous layers. These were eliminated by both the AUSM$^+$ and H-CUSP schemes.
2. Although the AUSM$^+$ and H-CUSP schemes have excellent shock capturing properties for model problems, all schemes gave comparable shock resolution on general grids.
3. The H-CUSP scheme usually predicted slightly lower total pressures (higher losses) than the other schemes.
4. There was no significant difference in convergence rates for the three schemes.
5. The C-D scheme has the lowest operation count and required the least CPU time of the three schemes. The H-CUSP scheme uses the same inviscid fluxes as the C-D scheme but has more complicated dissipative fluxes and is therefore slower. In both schemes the dissipative fluxes can be updated after the first one or two stages of a multistage Runge-Kutta scheme to save time. The AUSM$^+$ scheme has the highest operation count and was updated every stage, so it was the slowest of the three schemes. For a 2-D problem the H-CUSP scheme was 1.27 times slower than the C-D scheme and the AUSM$^+$ scheme was 2.6 times slower. For 3-D problems the viscous fluxes and turbulence models require disproportionately more time than the inviscid fluxes, so the AUSM$^+$ scheme requires relatively less of the overall time. For 3-D problems the H-CUSP scheme was 1.20 – 1.47 times slower than the C-D scheme and the AUSM$^+$ scheme was 1.24 – 1.57 times slower.
6. For a subsonic turbine vane the AUSM$^+$ and H-CUSP schemes predicted the 3-D wake shape better

than the C-D scheme. The AUSM$^+$ scheme gave the best overall predictions of turning and loss distributions.

7. For a transonic compressor rotor the AUSM$^+$ scheme predicted deficits in total pressure and total temperature that were measured experimentally but were not generally predicted by the C-D codes used for the ASME/AGARD test case. This result was consistent with predictions by Hah and Weber using two other upwind codes. We believe that the measured deficits in total pressure and total temperature are an intrinsic feature of this rotor blade and not a result of hub leakage as suggested by Shabbir, et al. Furthermore, we believe that C-D schemes tend to smear out these details due to relatively coarse spanwise grids, but that upwind schemes are able to capture them properly.

References

[1] Dunham, J., ed. "CFD Validation for Propulsion System Components," AGARD Advisory Report 355, AGARD, Nellie-Sur-Seine, France, May, 1998.

[2] Dunham, J., and Meauzé, "An AGARD Working Group Study of 3-D Navier-Stokes Codes Applied to Single Turbomachinery Blade Rows," ASME Paper 98-GT-50, June 1998.

[3] Reid, L., and Moore, R. D., "Design and Overall Performance of Four Highly-Loaded, High-Speed Inlet Stages for an Advanced, High-Pressure-Ratio Core Compressor," NASA TP-1337, 1978.

[4] Reid, L., and Moore, R. D., "Experimental Study of Low Aspect Ratio Compressor Blading," ASME Paper 80-GT-6, Mar. 1980.

[5] Tweedt, D. L., Chima, R. V., and Turkel, E. "Preconditioning for Numerical Simulation of Low Mach Number Three-Dimensional Viscous Turbomachinery Flows," AIAA Paper 97-1828, June, 1997.

[6] Chima, R. V., "A k-ω Turbulence Model for Quasi-Three-Dimensional Turbomachinery Flows," AIAA Paper 96-0248, 1995. Also NASA TM-107051.

[7] Jameson, A., Schmidt, W., and Turkel, E., "Numerical Solutions of the Euler Equations by Finite Volume Methods Using Runge-Kutta Time-Stepping Schemes," AIAA Paper 81-1259, June 1981.

[8] Martinelli, L., and Jameson, A., "Validation of a Multigrid Method for the Reynolds Averaged Equations," AIAA Paper 88-0414, Jan. 1988.

[9] Kunz, R. F., and Lakshminarayana, B. "Explicit Navier-Stokes Computation of Cascade Flows Using the k-ε Turbulence Model," *AIAA J.*, Vol. 30, No. 1, Jan. 1992, pp. 13-22.

[10] Tatsumi, S., Martinelli, L., and Jameson, A., "Design, Implementation, and Validation of Flux Limited Schemes for the Solution of the Compressible Navier-Stokes Equations," AIAA Paper 94-0647, Jan. 1994.

[11] Tatsumi, S., Martinelli, L., and Jameson, A., "A New High Resolution Scheme for Compressible Viscous Flows with Shocks," AIAA Paper 95-0466, Jan. 1995.

[12] Liou, M.-S., and Steffen, Jr., C. J., "A New Flux Splitting Scheme," *J. Computational Physics*, Vol. 107, No. 1, July 1993, pp. 23-39. ALSO NASA TM 104404, May 1991.

[13] Liou, M.-S., "A Sequel to AUSM: AUSM$^\pm$," *J. Computational Physics*, Vol. 129, 1996, pp. 364-382. Also NASA TM 106524, March 1994.

[14] Liou, M.-S., and Edwards, J. R., "Numerical Speed of Sound and its Application to Schemes for all Speeds," AIAA Paper 99-3268-CP, 14th AIAA CFD Conference, 1999. Also NASA TM-1999-209286, June 1999.

[15] Liou, M.-S., "Ten Years in the Making – AUSM-Family," AIAA Paper 2001-2521, June 2001.

[16] Chima, Rodrick V., "Explicit Multigrid Algorithm for Quasi-Three-Dimensional Viscous Flows in Turbomachinery," *AIAA Journal of Propulsion and Power*, Vol. 3, No. 5, Sept.-Oct. 1987, pp. 397-405.

[17] Chima, R. V., "Viscous Three-Dimensional Calculations of Transonic Fan Performance," in *CFD Techniques for Propulsion Applications*, AGARD Conference Proceedings No. CP-510, AGARD, Neuilly-Sur-Seine, France, Feb. 1992, pp 21-1 to 21-19. Also NASA TM-103800.

[18] Chima, Rodrick V., "Calculation of Tip Clearance Effects in a Transonic Compressor Rotor," ASME Paper 96-GT-114, June 1996. Also NASA TM-107216.

[19] Chima, Rodrick V., "Calculation of Multistage Turbomachinery Using Steady Characteristic Boundary Conditions," AIAA Paper 9800968, Jan. 1998. Also NASA TM-1998-206613.

[20] Baldwin, B. S., and Lomax, H., "Thin-Layer Approximation and Algebraic Model for Separated Turbulent Flows," AIAA Paper 78-257, Jan. 1978.

[21] Wilcox, D., C., *Turbulence Modeling for CFD*, DCW Industries, Inc., La Canada, CA, 1994.

[22] Menter, F. R., “Improved Two-Equation k-ω Turbulence Model for Aerodynamic Flows,” NASA TM-103975, Oct. 1992.

[23] Swanson, R. C., Radespiel, R., and Turkel, E., “Comparison of Several Dissipation Algorithms for Central Difference Schemes,” NASA-CR-201726, Aug. 1997. Also ICASE-97-40.

[24] van Albada, G. D., van Leer, B., and Roberts, W. W., “A Comparative Study of Numerical Methods in Cosmic Gas Dynamics,” ICASE Report No. 81-84, Aug. 1981.

[25] Arts, T., Lambert de Rouvroit, M., and Rutherford, A., W., “Aero-Thermal Investigation of a Highly Loaded Transonic Linear Turbine Guide Vane Cascade,” von Karman Institute Technical Note 174, Sept. 1990.

[26] Goldman, L. J., and McLallin, K. L., “Cold-Air Annular-Cascade Investigation of Aerodynamic Performance of Core-Engine-Cooled Turbine Vanes. I: Solid-Vane Performance and Facility Description,” NASA TM X-3224, 1975.

[27] Suder, K. L., and Celestina, M. L., “Experimental and Computational Investigation of the Tip Clearance Flow in a Transonic Axial Compressor Rotor,” NASA TM-106711, 1994.

[28] Suder, K. L., Chima, R. V., Strazisar, A. J., and Roberts, W. B., “The Effect of Adding Roughness and Thickness to a Transonic Axial Compressor Rotor,” ASME *J. Turbomachinery*, Vol. 117, Oct. 1995, pp 491-505.

[29] Hah, C. and Loellbach, J., “Development of Hub Corner Stall and its Influence on the Performance of Axial Compressor Blade Rows.,” ASME Paper 97-GT-42, June, 1997.

[30] Shabbir, A., Celestina, M. L., Adamczyk, J. J., and Strazisar, A. J., “The Effect of Hub Leakage Flow on Two High Speed Axial Compressor Rotors,” ASME Paper 97-GT-346, June 1997.

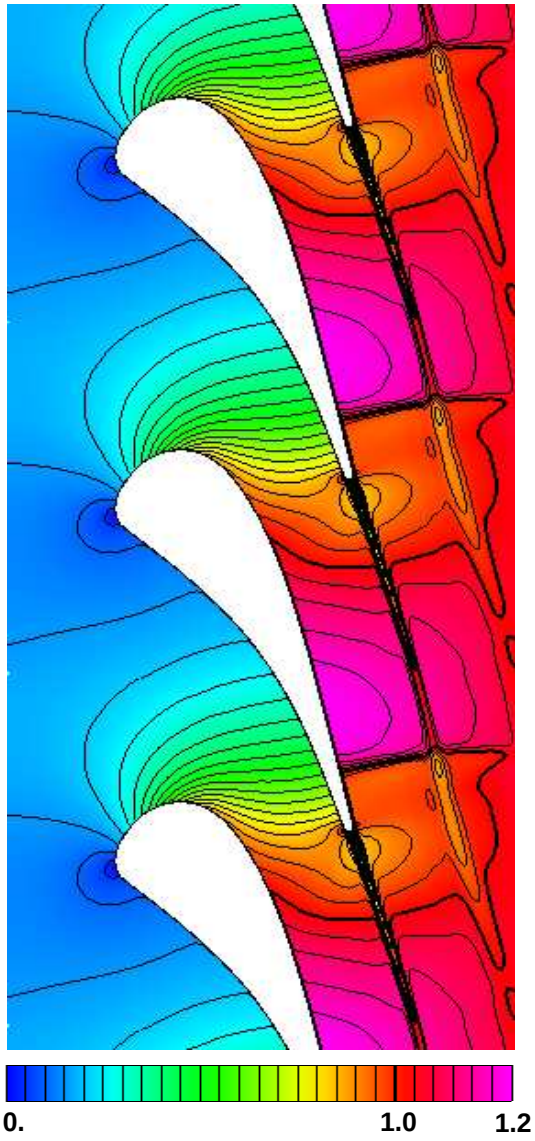

Figure 3 — Computed Mach contours for the VKI turbine vane, AUSM$^+$ scheme

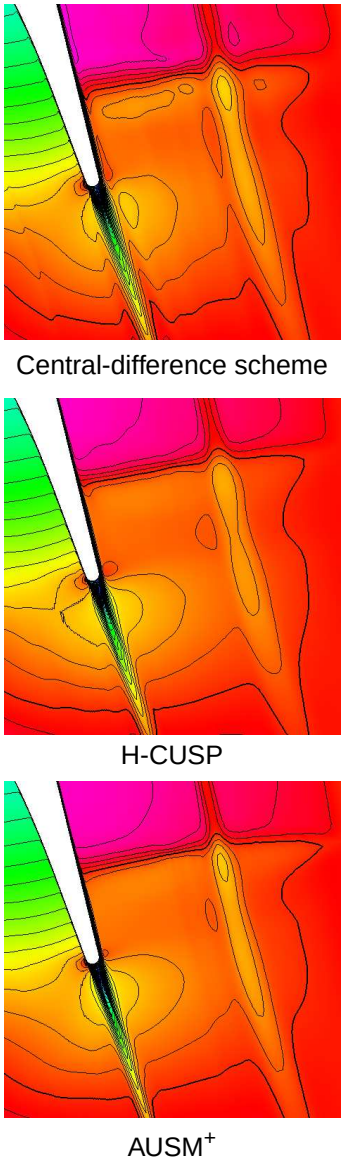

Figure 4 — Computed Mach contours at the trailing edge using three differencing schemes

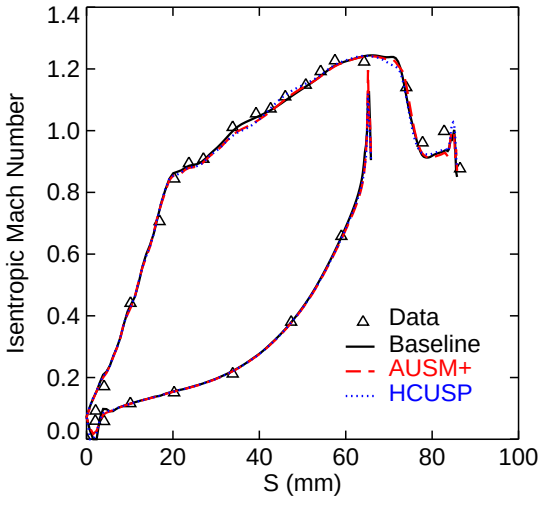

Figure 5 — Computed and measured distributions of isentropic Mach number on the vane surface

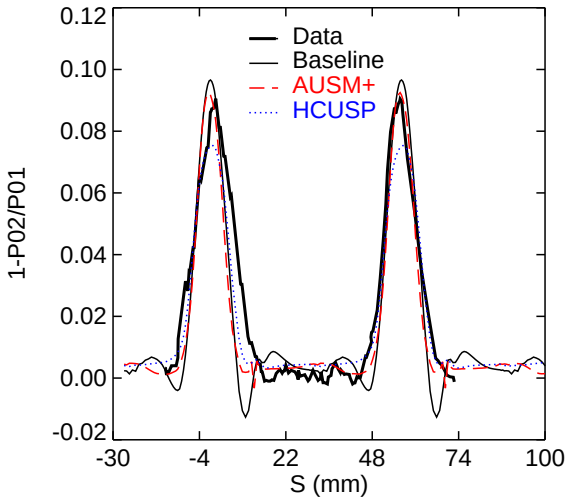

Figure 6 — Computed and measured total pressure profiles 0.43 chords behind the vane

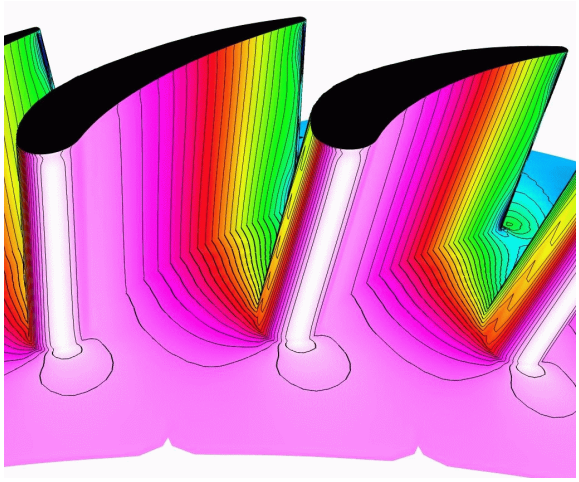

Figure 7 — Computed pressure contours on the Goldman turbine vane, AUSM$^+$ scheme

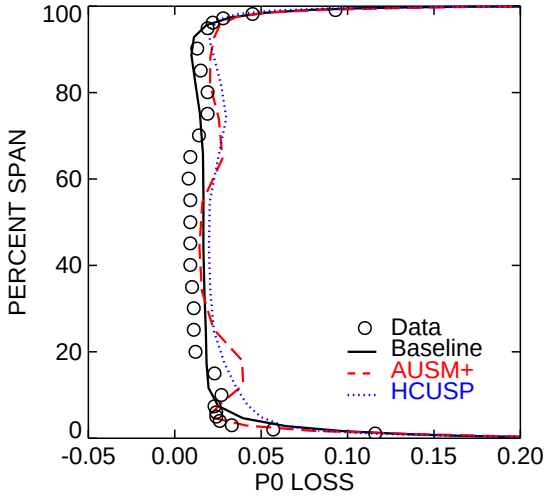

Figure 9 — Computed and measured profiles of P_0 loss coefficient downstream of the vane

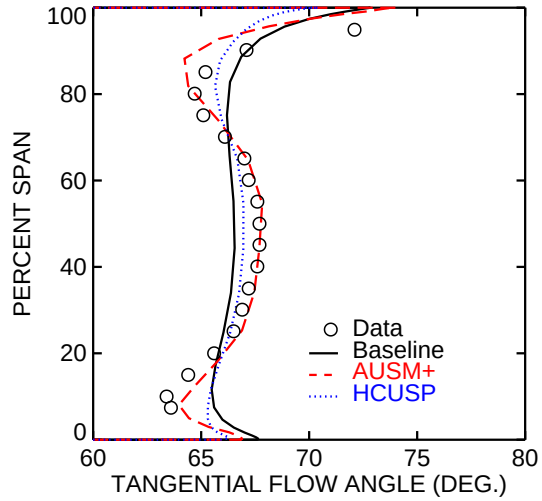

Figure 10 — Computed and measured profiles of flow angle downstream of the vane

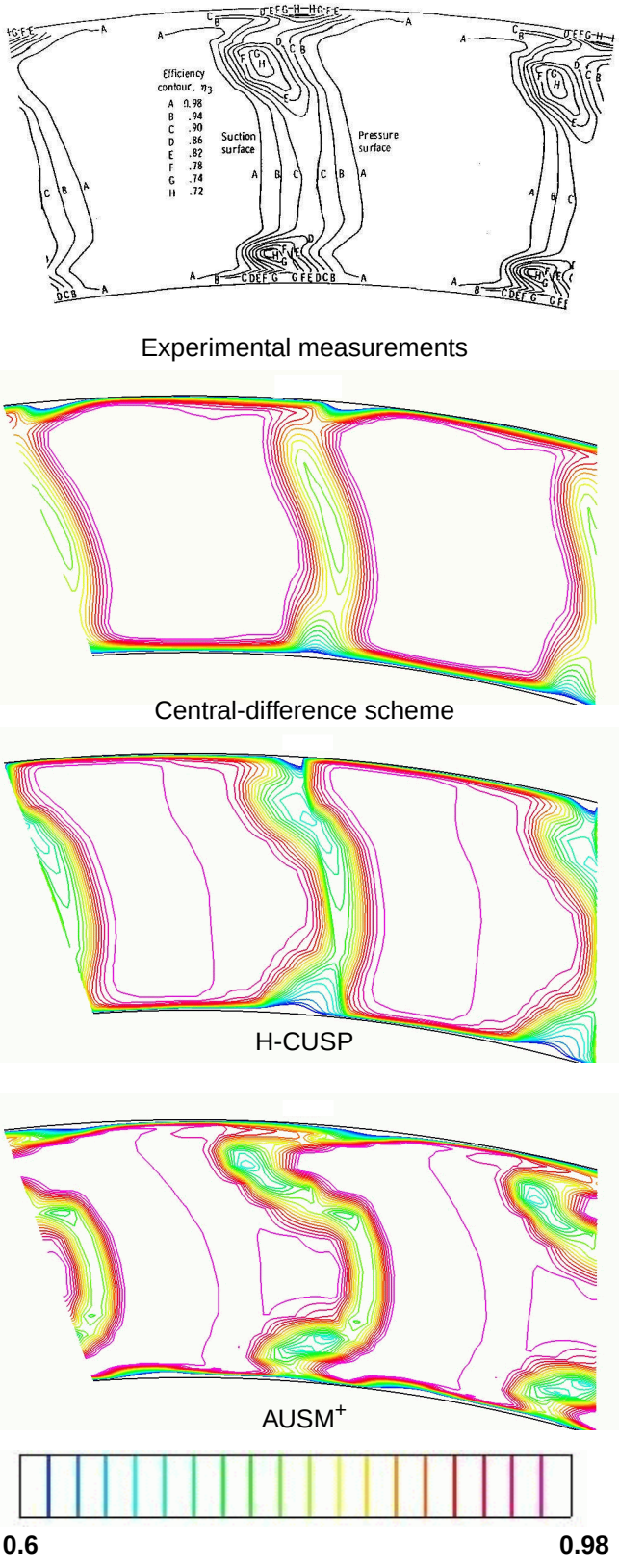

Figure 8 — Measured and computed profiles of kinetic energy efficiency in the vane wake

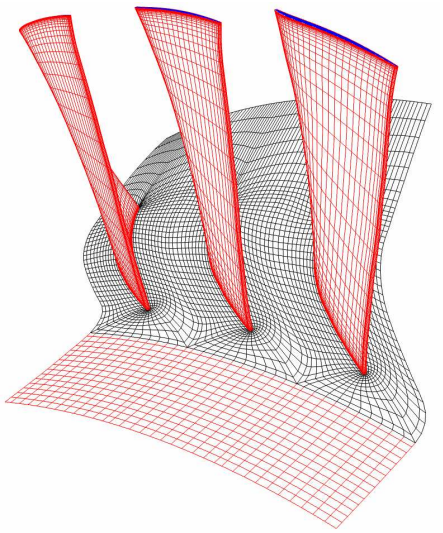

Figure 11 — Computational grid for NASA rotor 37

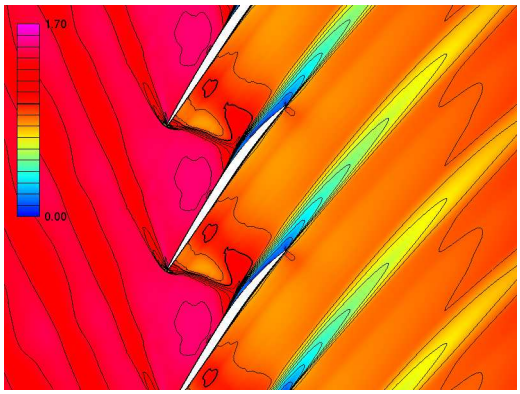

Figure 12 — Computed Mach contours at 73 percent span, AUSM$^+$ scheme

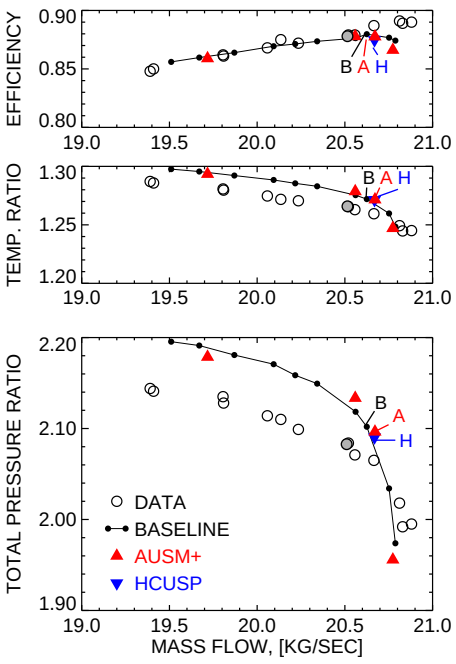

Figure 13 — Measured and computed operating maps of P_0, T_0, and η for rotor 37

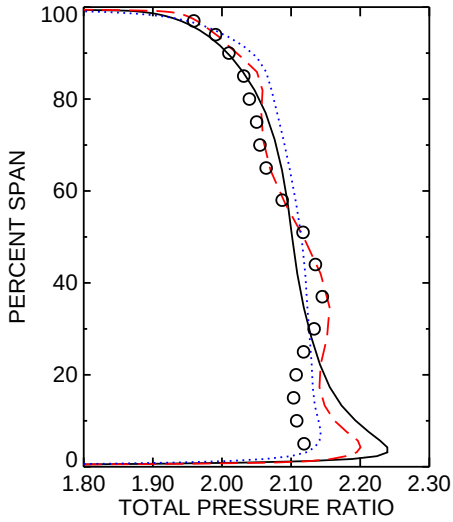

Figure 14 — Measured and computed profiles of total pressure downstream of the rotor

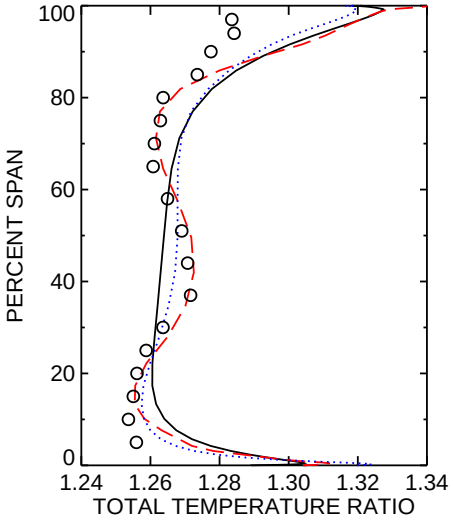

Figure 15 — Measured and computed profiles of total temperature downstream of the rotor

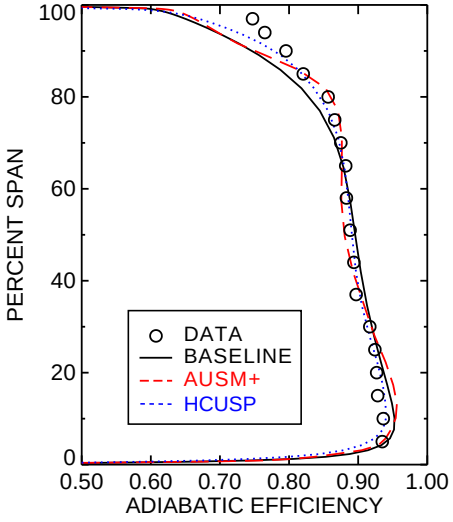

Figure 16 — Measured and computed profiles of adiabatic efficiency downstream of the rotor